This is the accepted manuscript made available via CHORUS. The article has been published as:

Evidence for a Quantum-to-Classical Transition in a Pair of Coupled Quantum Rotors

Bryce Gadway, Jeremy Reeves, Ludwig Krinner, and Dominik Schneble

Phys. Rev. Lett. **110**, 190401 — Published 7 May 2013

DOI: 10.1103/PhysRevLett.110.190401

Evidence for a quantum-to-classical transition in a pair of coupled quantum rotors

Bryce Gadway,* Jeremy Reeves, Ludwig Krinner, and Dominik Schneble
Department of Physics and Astronomy, Stony Brook University, Stony Brook, NY 11794-3800, USA

The understanding of how classical dynamics can emerge in closed quantum systems is a problem of fundamental importance. Remarkably, while classical behavior usually arises from coupling to thermal fluctuations or random spectral noise, it may also be an innate property of certain isolated, periodically driven quantum systems. Here, we experimentally realize the simplest such system, consisting of two coupled quantum kicked rotors, by subjecting a coherent atomic matter wave to two periodically pulsed, incommensurate optical lattices. Momentum transport in this system is found to be radically different from that in a single kicked rotor, with a breakdown of dynamical localization and the emergence of classical diffusion. Our observation, which confirms a long-standing prediction for many-dimensional quantum-chaotic systems, sheds new light on the quantum-classical correspondence.

PACS numbers: 67.85.Hj ; 05.45.Mt ; 61.43.-j

In ultracold atomic systems, the quantum nature of matter can be made manifest in striking ways. One example arises in the dynamics of quantum chaotic systems [1], i.e. in systems whose classical counterparts are chaotic and in which destructive interference can suppress the onset of chaos. A paradigm model, the δ-kicked rotor (δ-KR), can been realized with atomic matter waves subject to a periodically pulsed optical lattice [2]. Whereas regimes of fully chaotic behavior with diffusive growth of the momentum variable are expected in the classical case, destructive interference leads to dynamical localization [3–5] for which the momentum distribution remains frozen. The phenomenon of dynamical localization in the δ-KR is a direct analog of real-space Anderson localization in one-dimensional (1D) disordered materials [6], and recent experimental work [7–10] based on a generalization to quasi-periodic kicking [11] has also provided access to the three-dimensional case.

Several experimental studies of the δ-KR model [12–17] have focused on the degradation of dynamical localization in the presence of noise [11, 18–20] and nonlinearities [21–23]. Remarkably, signatures of classical behavior have been predicted [21] to emerge already in a simple driven quantum system consisting of just two coupled kicked rotors, providing hope that the disparate behavior of quantum and classically chaotic systems may be reconciled in the macroscopic limit.

In this paper we realize such a simple coupled quantum system by subjecting a macroscopic matter wave to two periodically pulsed, incommensurate optical lattices [24]. As detailed further below, the coupling between the two rotors, each separately driven by one of the lattices, arises from the kinetic evolution between the pulses. We find that the coupling destroys hallmark behavior of the off-resonantly driven δ-KR system, causing a transition from dynamical localization to classically diffusive momentum-space transport. Additionally, we observe that the coupling greatly modifies the response of atoms to resonant driving, leading to a suppression of ballistic transport in momentum space.

Our system consists of an optically-trapped Bose-Einstein condensate of $(1.4\pm0.4)\times10^5$ ^{87}Rb atoms in the $|F, m_F\rangle = |2, -2\rangle$ hyperfine ground state, which is subject to two simultaneously pulsed, incommensurate optical lattices [24] along z, as depicted in Fig. 1 (a). The lattices have wavelengths $\lambda_1 = 1064$ nm and $\lambda_2 = 782$ nm

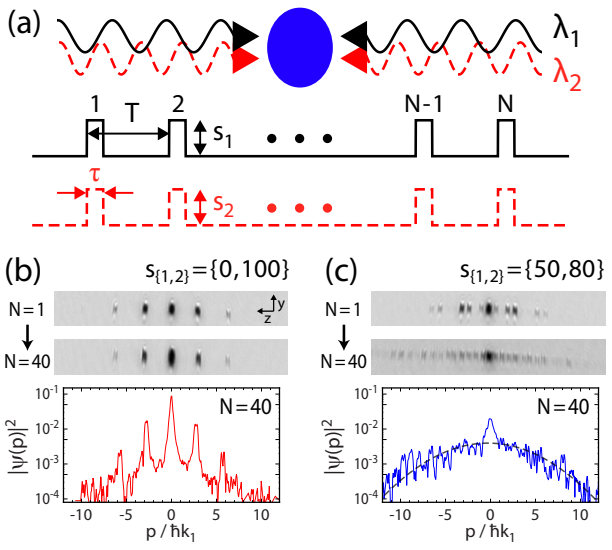

FIG. 1. Atomic matter waves in a periodically pulsed optical lattice potential. (a) A Bose–Einstein condensate is exposed to a train of N pulses (duration τ, separation T) of two incommensurate optical lattices (wavelengths $\lambda_{1,2}$ and depths $s_{\{1,2\}}$). (b) Time-of-flight diffraction spectra (averaged over 3-4 images) of atoms released after $N = 1$ and 40 kicks, for driving with a single lattice ($s_{\{1,2\}} = \{0, 100\}$). The momentum distribution along z (integrated along y) after $N = 40$ kicks is shown in the bottom. (c) As in (b), but for driving with two incommensurate lattices ($s_{\{1,2\}} = \{50, 80\}$). The dashed black line at the bottom of (c) is a Gaussian profile corresponding to diffusive spreading.

(wave numbers $k_{1(2)} = 2\pi/\lambda_{1(2)}$) and lattice depths $s_{1(2)}E_R$, where $E_R = \hbar^2 k_1^2/2M$ is the recoil energy of the first lattice and M the atomic mass. The pulses have a duration $\tau = 2$ μs (Raman–Nath regime) and are spaced at a variable period T. After applying N pulses, we immediately release the atoms and allow them to freely evolve in time-of-flight for 16 ms before performing absorptive imaging of momentum distributions, with examples shown in Figs. 1 (b,c).

Ignoring effects of the trapping potential and atom-atom interactions, this system can be approximately described by the 1D Hamiltonian $H = -\hbar^2\partial_z^2/2M + S(z)\sum_{j=1}^{N}\sqcap(t/\tau - jT/\tau)$, where $S(z) = [s_1\cos(2k_1 z) + s_2\cos(2\eta k_1 z)]E_R/2$, $\sqcap$ is the normalized boxcar function, and $\eta = k_2/k_1 \sim 1.36$ is the ratio of wavenumbers. Diffraction by the two optical lattices connects the zero-momentum condensate to modes with momenta in multiples of $2\hbar k_1$ and $2\eta\hbar k_1$, respectively. The two sets of modes have no intersection for irrational values of η, which allows us to describe the system as effectively 2D in the plane wave basis $|m,n\rangle = |m\rangle \bigotimes |n\rangle$, with momenta $p_{m,n} = 2(m+\eta n)\hbar k_1$ (we assume that the mode separation exceeds the spectral width of the condensate).

Approximating the lattice pulses as δ-functions, the effective 2D Hamiltonian for the system is given by

$$H = H_T + \hbar(\hat{\phi}_{V_1} + \hat{\phi}_{V_2})\sum_{j=1}^{N}\delta(t - jT)\ , \qquad (1)$$

where $H_T = \hbar/T\sum_{m,n} D_{m,n}\hat{n}_{m,n}$ describes the kinetic energy of the plane-wave modes with

$$D_{m,n} = \kappa(m^2/2 + \eta mn + \eta^2 n^2/2)\ , \qquad (2)$$

and the effect of the pulsed optical potential is captured by

$$\hat{\phi}_{V_{1(2)}} = (K_{1(2)}/\kappa)\sum_{m,n}(\hat{\sigma}^{-,1(2)}_{m,n} + \hat{\sigma}^{+,1(2)}_{m,n})\ , \qquad (3)$$

where $\hat{\sigma}^{\pm,1}_{m,n} = \hat{a}^\dagger_{m\pm1,n}\hat{a}_{m,n}$ and $\hat{\sigma}^{\pm,2}_{m,n} = \hat{a}^\dagger_{m,n\pm1}\hat{a}_{m,n}$ describe transitions within each set of modes. Here, $\hat{a}^\dagger_{m,n}$ ($\hat{a}_{m,n}$) is the creation (annihilation) operator and $\hat{n}_{m,n}$ is the number operator of the composite mode $|m,n\rangle$. As in the standard treatment of the δ-KR [2], which is realized when either lattice is pulsed alone, we define $\kappa = 8E_R T/\hbar$ and $K_{1(2)} = \kappa s_{1(2)}E_R\tau/2\hbar$. Here, the single-rotors are driven resonantly whenever $\kappa/4\pi$ ($\eta^2\kappa/4\pi$) is a rational number, i.e. whenever the frequency of δ-kicking matches a Talbot resonance [25, 26], and the stochasticity parameters $K_{1(2)}$ delineate regimes of regular and chaotic motion in the classical δ-KR model.

A simple picture of the δ-KR and its connection to the Anderson model emerges from a stroboscopic Floquet analysis [6], in which the effect of each kick is described by the operator $\hat{U} = \exp[-i(\hat{\phi}_{V_1} + \hat{\phi}_{V_2})]\exp[-i\sum_{m,n} D_{m,n}\hat{n}_{m,n}]$, such that the initial state $|\psi_0\rangle = |m=0, n=0\rangle$ is transformed to $|\psi_N\rangle = \hat{U}^N|\psi_0\rangle$ after a series of N kicks. The term $D_{m,n}$ (taken modulo 2π) contained in the operator $\hat{U}$ describes the kinetic phase evolution between kicks. In the language of the Anderson model, it represents a 2D quasienergy landscape, within which the terms $K_{1(2)}/\kappa$ control the strength of discrete-time hopping.

We first discuss a single rotor at quantum resonance, which is obtained e.g. for the first lattice when $\kappa/4\pi$ is a rational number. In this case, the relevant quasienergy term from Eq. 2 is equal to zero (mod 2π) for all of the momentum orders, corresponding to a flat quasienergy landscape in which tunneling occurs. Thus, atoms initially localized to a single momentum mode will undergo ballistic momentum-space transport [25, 26] corresponding to a quantum walk [27]. Contrastingly, if the resonance condition is not fulfilled, the quasienergy landscape is characterized by pseudorandom disorder in which the atomic wavefunction dynamically localizes [2].

In our case of two kicked rotors, the 2D quasienergy landscape is anisotropic. The quantities $\kappa/2$ and $\eta^2\kappa/2$ control the disorder strengths in the two directions, and in the absence of the coupling, this 2D system should display localization for any finite disorder strength [28]. However, in our system a coupling between the ro-

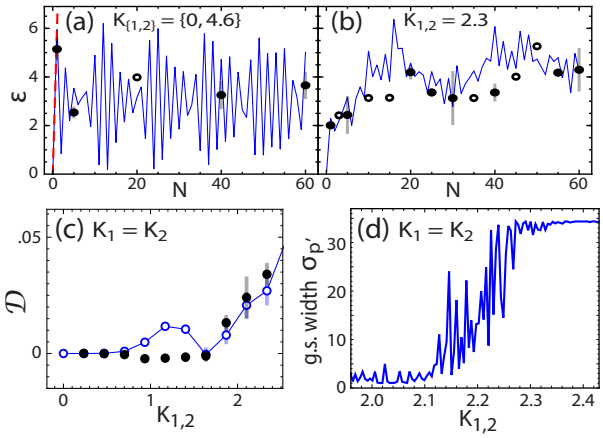

FIG. 2. Matter-wave dynamics for off-resonant kicking. (a) Kicking by a single lattice, with $K_2 = 4.6$. Shown is the atoms' per-particle energy ε as a function of kick number N. The black points are experimental data with statistical error bars (empty circles for individual runs) while the blue solid and red dashed lines are simulated quantum and classical trajectories. (b) Off-resonant kicking with two incommensurate lattices ($K_1 = K_2 = 2.3$). (c) Energy diffusion rates, $\mathcal{D} = \Delta\varepsilon/\Delta N$, as determined from linear fits to data and simulated points as in (b), as a function of the kicking strength for the uniform case $K_1 = K_2 \equiv K_{1,2}$. Filled black points are experimental, open blue disks represent numerical, and error bars represent the standard error of the linear fits. (d) Calculated rms momentum width $\sigma_{p'}$ (in units $\hbar k_1$) for the ground state of the single-kick Floquet operator $\hat{U}$.

tors arises because the geometry remains physically one-dimensional and because the free-space dispersion relation for massive particles is quadractic. In the following, we shall investigate the effect of the coupling term $\kappa\eta mn$ in Eq. 2 on the localization properties of the system.

In our experiment, we first tune the pulse period T such that the kicking is off-resonant for both lattices ($T = 36\ \mu$s; $\kappa/4\pi \approx 0.29$; $\eta^2\kappa/4\pi \approx 0.54$). In the single-lattice case, the atomic population remains trapped in the lowest momentum orders and the per-particle energy ε (in units of E_R) shows no net increase over a large number of pulses, as shown in Fig. 1 (b) and Fig. 2 (a) for $K_{\{1,2\}} = \{0, 4.6\}$, in agreement with the expectation for dynamical localization, which occurs after a "quantum break time" $t_B = TK^2/4\kappa^2$ [2, 13]. For our system parameters, t_B is smaller than T (similar as in [17]), such that dynamical localization sets in immediately. This finding is confirmed by an exact numerical simulation in the plane wave basis of states $|m, n\rangle$ with momentum $p_{m,n} = 2(m + \eta n)\hbar k_1$ which displays a fast oscillatory behavior around a constant mean energy [29]. The lack of growth is also in stark contrast to computed classical trajectories, whose energy increases very rapidly, cf. Fig. 2 (a), ruling out effects of classical localization [30].

In contrast to the behavior seen for off-resonant kicking with a single lattice, we observe a delocalization of the atomic population into a nearly Gaussian momentum distribution when the second such lattice is added. This is shown in Fig. 1 (c) for $K_{\{1,2\}} = \tilde{K} = \{2.3, 3.7\}$. For uniform kicking $K_1 = K_2 \equiv K_{1,2}$, we observe a threshold near $K_{1,2} \sim 2$ [cf. Fig. 2 (b,c)], above which dynamical localization disappears and energy growth sets in. This finding is reproduced by the ground-state properties of the single-kick operator $\hat{U}$, for which a time-independent stroboscopic Floquet state analysis [6, 9] reveals a transition from localized to delocalized states at $K_{1,2} \sim 2.2$, cf. Fig. 2 (d).

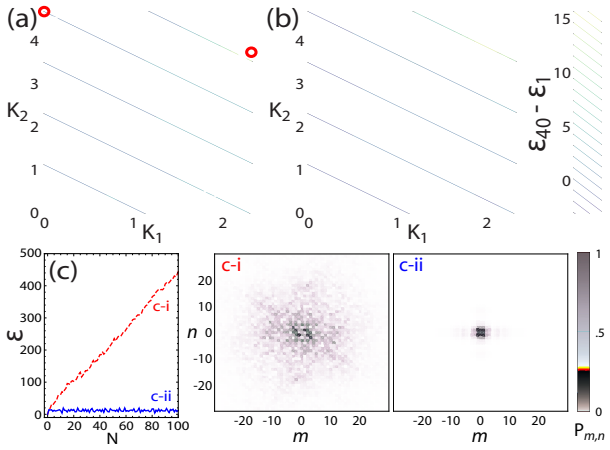

FIG. 3. Delocalization of coupled kicked quantum rotors in two dimensions. (a,b) Measured and simulated change in ε between $N = 1$ to 40 kicks as a function of K_1 and K_2 (8-9 sampled points in each direction), for off-resonant kicking as in Fig. 2. The circles labeled 1-b and 1-c highlight data derived from the distributions shown in Figs. 1 (b,c). (c) Simulated dependence of the energy ε on N for off-resonant δ-kicking ($T = 36\ \mu$s ; $\tau = 10$ ns) by two equally deep lattices of $K_{1,2} = 5.8$, with (c-i, red dashed line) and without (c-ii, blue solid line) the cross-coupling term of $D_{m,n}$. At right, 2D momentum distributions after $N = 100$ kicks, decomposed with respect to the two lattices ($\mathrm{P}_{m,n} = |\langle m, n|\psi_N\rangle|^2$).

The full dependence of the observed growth on the kicking strengths K_1 and K_2 is shown in Fig. 3 (a). We find essentially zero growth along the axes when either of the lattices are off-resonantly kicked alone, and a transition to diffusive growth when there is significant kicking by both lattices. The data are in good agreement with simulated quantum trajectories [29], cf. Fig. 3 (b), including the position of maximal growth near $\tilde{K}$. While the coupling term $\kappa\eta mn$ responsible for delocalization cannot be independently accessed in our experimental geometry, we can verify its role through numerical simulations as in Fig. 3 (c), which can also probe more deeply into the diffusive, metallic phase. A linear energy growth, characteristic of diffusive transport, is clearly seen for strong kicking as a consequence of the coupling term, as opposed to a complete suppression of growth in its absence. The simulated growth is found to be very stable [29], persisting to timescales over 3 orders of magnitude longer than the system's quantum break time t_B (limited only by the simulated system size). Furthermore, we find that in the limit of strong uniform driving the energy diffusion rate $\mathcal{D} = \Delta\varepsilon/\Delta N$ is not only nonzero, but asymptotically approaches the classical diffusion rate $\mathcal{D}_c = 2(1 + \eta^2)K_{1,2}^2/\kappa^2$ [29].

We note that there exist fundamental differences between our observations and recent experimental investigations of the 3D Anderson model with cold atomic vapors driven at more than one frequency [7, 8, 10], where a metal to insulator transition results from the competition between disorder and tunneling. Driving a single lattice at multiple temporal frequencies [11, 31] is equivalent to a scenario of multiple uncoupled rotors. In contrast, we observe a transition in 2D that critically depends on the inter-rotor coupling. The term $\kappa\eta mn$ in Eq. 2 represents a saddle potential which, when added to the two quadratic terms, breaks reflection symmetry about either of the two axes ($m \to -m$ and $n \to -n$), and on average breaks the $\mathbb{Z}_4$ rotational symmetry of the potential landscape. We point out that the observed coupling-induced diffusive behavior is particular to the pseudo-randomness of disorder in the δ-KR system, and that it is not seen in simulations when purely random diagonal disorder is used instead. This is consistent with the fact that transitions from insulating to metallic behavior do not occur in 2D systems with purely random disorder, absent the breaking of time-reversal symmetry or spin-rotation invariance [32–34] (as due to strong magnetic fields or

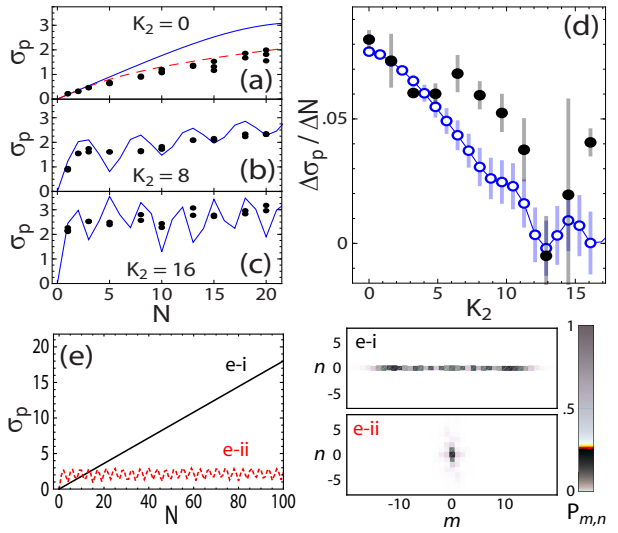

FIG. 4. Dynamical evolution of resonantly kicked matter waves ($K_1 = 1.6$) in the presence an additional off-resonant drive (K_2). (a,b,c) Momentum-width σ_p of the atomic distribution as a function of kick number N, for a pulse period $T = 124$ μs ($\kappa/4\pi \approx 1$), and $K_2 = 0, 8, 16$. Black points are data from individual experimental runs, the blue line is a numerical calculation for an initial plane-wave, while the dashed red curve takes into account finite-size corrections [29]. (d) Growth rate of the momentum-width $\Delta\sigma_p/\Delta N$, determined by a linear fit to the N-dependence, as a function of K_2. The simulated growth rates (open blue circles) are scaled by a factor of 1/2 to account for effects of finite size. (e) Dependence of the momentum width σ_p on kick number N, for the case of resonant kicking ($\kappa/4\pi = 1$; $\tau = 10$ ns) with a single lattice ($K_{\{1,2\}} = \{1.6, 0\}$, black solid line e-i), and with an added deep incommensurate lattice ($K_{\{1,2\}} = \{1.6, 12.8\}$, red dashed line e-ii). Characteristic momentum-space profiles in the 2D m-n space are shown at right for $N = 100$.

spin-orbit coupling in electronic systems).

Finally, we study our system at a quantum resonance of one of the rotors. For this purpose, we set $\kappa/4\pi \approx 1$ ($T = 124$ μs) for the first lattice, while keeping the second lattice off-resonant ($\eta^2\kappa/4\pi \approx 1.86$). When the second lattice is off, we observe a linear increase in the rms momentum width σ_p (in units of $\hbar k_1$), cf. Fig. 4 (a). This is expected for constructive interference and characteristic of ballistic momentum-space transport. Adding the second lattice causes a reduction of the observed growth rate, depending on the strength of this lattice, cf. Figs. 4 (b,c,d). To elucidate the mechanism behind this decrease, we show in Fig. 4 (e) simulations for a larger number of kicks (and for more ideal δ-kicking exactly at resonance). The dynamics of σ_p and the distributions of population within the 2D m-n space suggest that the inhibition of ballistic transport is due not to a crossover to classical diffusion ($\sigma_p \propto \sqrt{N}$) as seen in the off-resonant case, but rather to the onset of dynamical localization in the strongly driven incommensurate lattice. The obvious underlying cause for the suppression is again the coupling term $\kappa\eta mn$, which destroys coherent phase revival between kicks. Remarkably, a complete suppression of resonant growth results even though the population spends nearly half of its time in the $n = 0$ subspace, where the coupling vanishes. This dynamical suppression of resonant quantum transport due to the admixture of off-resonant driving bears some resemblance to effects seen in other dynamical systems such as the Kapitza pendulum or ponderomotive potentials acting on charged particles.

To conclude, we have experimentally observed a quantum-to-classical transition from localized to delocalized dynamics in a system of coupled quantum kicked rotors. Further studies of our model system, as well as extensions to larger numbers of coupled rotors using several mutually incommensurate optical lattices, might help to provide insight into localization phenomena in nonlinear and disordered systems.

We thank Alexander Altland and Mikael Rechtsman for discussions, and Martin G. Cohen and Thomas Bergeman for comments on the manuscript. This work was supported by NSF (PHY-0855643). B.G. and J.R. acknowledge support from the GAANN program of the US DoEd.

* present address: JILA, University of Colorado, 440 UCB, Boulder, CO 80309-0440

[1] F. Haake, *Quantum Signatures of Chaos*, 3rd ed. (Springer, 2010).
[2] F. L. Moore *et al.*, Phys. Rev. Lett. **75**, 4598 (1995).
[3] G. Casati *et al.*, "Stochastic behavior in classical and quantum hamiltonian systems," (Springer, New York, 1979) p. 334.
[4] T. Hogg and B. A. Huberman, Phys. Rev. Lett. **48**, 711 (1982).
[5] S. Fishman, D. R. Grempel, and R. E. Prange, Phys. Rev. Lett. **49**, 509 (1982).
[6] D. R. Grempel, R. E. Prange, and S. Fishman, Phys. Rev. A **29**, 1639 (1984).
[7] J. Ringot *et al.*, Phys. Rev. Lett. **85**, 2741 (2000).
[8] J. Chabé *et al.*, Phys. Rev. Lett. **101**, 255702 (2008).
[9] G. Lemarié *et al.*, Phys. Rev. A **80**, 043626 (2009).
[10] G. Lemarié *et al.*, Phys. Rev. Lett. **105**, 090601 (2010).
[11] G. Casati, I. Guarneri, and D. L. Shepelyansky, Phys. Rev. Lett. **62**, 345 (1989).
[12] H. Ammann, R. Gray, I. Shvarchuck, and N. Christensen, Phys. Rev. Lett. **80**, 4111 (1998).
[13] B. G. Klappauf *et al.*, Phys. Rev. Lett. **81**, 1203 (1998).
[14] M. B. d'Arcy *et al.*, Phys. Rev. Lett. **87**, 074102 (2001).
[15] M. B. d'Arcy *et al.*, Phys. Rev. E **64**, 056233 (2001).
[16] C. Zhang *et al.*, Phys. Rev. Lett. **92**, 054101 (2004).
[17] G. J. Duffy *et al.*, Phys. Rev. A **70**, 041602 (2004).
[18] D. L. Shepelyansky, Physica **8D**, 208 (1983).
[19] E. Ott, T. M. Antonsen, and J. D. Hanson, Phys. Rev. Lett. **53**, 2187 (1984).
[20] R. Graham and A. R. Kolovsky, Physics Letters A **222**, 47 (1996).

[21] S. Adachi, M. Toda, and K. Ikeda, Phys. Rev. Lett. **61**, 659 (1988).
[22] F. Benvenuto *et al.*, Phys. Rev. A **44**, R3423 (1991).
[23] D. L. Shepelyansky, Phys. Rev. Lett. **70**, 1787 (1993).
[24] G. Roati *et al.*, Nature **453**, 895–898 (2008).
[25] L. Deng *et al.*, Phys. Rev. Lett. **83**, 5407 (1999).
[26] C. Ryu *et al.*, Phys. Rev. Lett. **96**, 160403 (2006).
[27] A. Romanelli *et al.*, Physica A **352**, 409 (2005); A. Romanelli, R. Siri, and V. Micenmacher, Phys. Rev. E **76**, 037202 (2007).
[28] E. Abrahams, P. W. Anderson, D. C. Licciardello, and T. V. Ramakrishnan, Phys. Rev. Lett. **42**, 673 (1979).
[29] See Supplementary Material for more information on the theoretical analysis.
[30] T. Geisel, G. Radons, and J. Rubner, Phys. Rev. Lett. **57**, 2883 (1986).
[31] C. Tian, A. Altland, and M. Garst, Phys. Rev. Lett. **107**, 074101 (2011).
[32] J. Bellissard, D. R. Grempel, F. Martinelli, and E. Scoppola, Phys. Rev. B **33**, 641 (1986).
[33] S. N. Evangelou, Phys. Rev. Lett. **75**, 2550 (1995).
[34] F. Evers and A. D. Mirlin, Rev. Mod. Phys. **80**, 1355 (2008).